Deformation of the Lamina Cribrosa and Optic Nerve Due to Changes in Cerebrospinal Fluid Pressure

Andrew J. Feola,[1] Baptiste Coudrillier,[1,2] John Mulvihill,[1,3] Diogo M. Geraldes,[4] Nghia T. Vo,[5] Julie Albon,[6,7] Richard L. Abel,[8] Brian C. Samuels,[9] and C. Ross Ethier[1]

[1]Department of Biomedical Engineering, Georgia Institute of Technology/Emory University, Atlanta, Georgia, United States
[2]Exponent, Inc., Menlo Park, California, United States
[3]School of Engineering/Bernal Institute, University of Limerick, Limerick, Ireland
[4]Biomechanics Group, Department of Mechanical Engineering, Imperial College London, London, United Kingdom
[5]Diamond Light Source, Didcot, United Kingdom
[6]Optic Nerve Group, School of Optometry and Vision Sciences, Cardiff University, Cardiff, Wales, United Kingdom
[7]Cardiff Institute of Tissue Engineering and Repair, Cardiff University, Cardiff, Wales, United Kingdom
[8]Department of Surgery and Cancer, Imperial College, London, United Kingdom
[9]Department of Ophthalmology, University of Alabama at Birmingham, Birmingham, Alabama, United States

PURPOSE. Cerebrospinal fluid pressure (CSFp) changes are involved or implicated in various ocular conditions including glaucoma, idiopathic intracranial hypertension, and visual impairment and intracranial pressure syndrome. However, little is known about the effects of CSFp on lamina cribrosa and retrolaminar neural tissue (RLNT) biomechanics, potentially important in these conditions. Our goal was to use an experimental approach to visualize and quantify the deformation of these tissues as CSFp increased.

METHODS. The posterior eye and RLNT of porcine eyes ($n = 3$) were imaged using synchrotron radiation phase-contrast micro-computed tomography (PC μCT) at an intraocular pressure of 15 mm Hg and CSFps of 4, 10, 20, and 30 mm Hg. Scans of each tissue region were acquired at each CSFp step and analyzed using digital volume correlation to determine 3-dimensional tissue deformations.

RESULTS. Elevating CSFp increased the strain in the lamina cribrosa and RLNT of all three specimens, with the largest strains occurring in the RLNT. Relative to the baseline CSFp of 4 mm Hg, at 30 mm Hg, the lamina cribrosa experienced a mean first and third principal strain of 4.4% and −3.5%, respectively. The corresponding values for the RLNT were 9.5% and −9.1%.

CONCLUSIONS. CSFp has a significant impact on the strain distributions within the lamina cribrosa and, more prominently, within the RLNT. Elevations in CSFp were positively correlated with increasing deformations in each region and may play a role in ocular pathologies linked to changes in CSFp.

Keywords: cerebrospinal fluid pressure, digital volume correlation, intracranial pressure, ocular biomechanics, phase-contrast micro-computed tomography

The optic nerve head (ONH) experiences a complex and dynamic biomechanical environment, with ONH tissues being exposed to several levels of pressure, in addition to blood pressure: anteriorly, they experience intraocular pressure (IOP), while posteriorly they experience retrolaminar tissue pressure and cerebrospinal fluid pressure (CSFp). Intraocular pressure retro-displaces ONH tissues and also generates stress on the entire corneoscleral shell, increasing the in-wall circumferential stress ("hoop stress") within this shell. This stress results in scleral canal expansion, which contributes to lamina cribrosa deformation.[1–4] The biomechanical forces created by IOP are partially opposed by the retrolaminar tissue pressure, which is modulated by CSFp when CSFp is greater than 0 mm Hg.[5]

It is thought that biomechanics play a role in glaucomatous optic neuropathy.[2,6] Thus, we and others have investigated the effects of IOP on ONH biomechanics by using both experi-mental and computational approaches.[7–11] The effects of CSFp on ONH biomechanics have more recently begun to receive significant attention for several reasons. First, although elevated IOP is a major risk factor for developing glaucoma, reduced CSFp has also been implicated in the disease.[12–15] In addition, elevated CSFp is associated with other ocular pathologies: hypothetically it plays a role in visual impairment and intracranial pressure (VIIP) syndrome and is, by definition, involved in the ocular changes associated with idiopathic intracranial hypertension (IIH).[16,17] Both patients with IIH and astronauts with VIIP syndrome share certain pathologic characteristics, including disc edema, optic nerve sheath kinking, and choroidal folds.[16–19]

Previous experimental work by Morgan et al.[20] examined the movement of the optic disc surface as a function of IOP or CSFp. Using a canine model, that study controlled IOP and CSFp by cannulating the anterior chamber and lateral ventricles, respec-

tively. Relative changes in the optic disc location were measured using confocal scanning laser tomography. The authors reported that changes in CSFp caused large displacements of the optic disc surface with only a 2-mm Hg increase of CSFp, causing a 128-μm movement of the optic disc surface. That work highlighted how CSFp could directly impact the displacement of ONH tissues. However, due to light penetration limitations, the authors were unable to directly image motion of the lamina cribrosa or retrolaminar neural tissue (RLNT). In addition, although they measured relative displacement of the optic disc surface, that approach did not have the resolution to determine tissue strain; this is an important point because it is believed that cells are mechanically sensitive to strain,[21,22] yet strain and displacement are not the same. Specifically, "strain" refers to stretching, compression, and/or shear deformations, types of movement that are fundamentally different from, for example, rigid body displacement, where an object moves without deformation. Complex tissue motions, such as anterior-posterior optic disc movement, will include both rigid body displacement and strain, and it is not a trivial matter to separate these contributions.

Recent computational modeling studies have investigated how elevations in CSFp affect the biomechanics of the ONH, including the lamina cribrosa and RLNT.[23] These studies found that elevating CSFp increased biomechanical strains in the RLNT while decreasing strains in the lamina cribrosa. Although these results make intuitive sense, these complex computational models must make many assumptions about tissue behavior and ONH geometries. Thus, it is important to develop experimental protocols to help verify findings in these computational studies and better characterize how CSFp affects deformations at the ONH. In the present study we describe high-resolution imaging experiments to investigate how CSFp deforms the lamina cribrosa and RLNT. We hypothesized that elevating CSFp would increase the strains experienced by the RLNT while decreasing the strains in the lamina cribrosa.

METHODS

Overview

We used phase-contrast micro-computed tomography (PC μCT) to measure CSFp-induced deformations of the lamina cribrosa and RLNT. Imaging was carried out at the Diamond Light Source synchrotron (Didcot, UK), a facility with phase-contrast imaging capability, which provides label-free images of ocular connective tissues at high spatial resolution.[24,25] Postmortem porcine eyes were prepared to allow independent control over IOP and CSFp. Then, while holding IOP constant (15 mm Hg), we elevated CSFp stepwise and recorded images of the lamina cribrosa and RLNT. From these images, we determined tissue strains in a post processing step.

This methodology allowed us to investigate the influence of CSFp on the lamina cribrosa and RLNT without limitations of light attenuation (e.g., such as occur in confocal scanning laser tomography and optical coherence tomography) and without tissue preparation that might have influenced ONH biomechanics (e.g., conventional μCT).
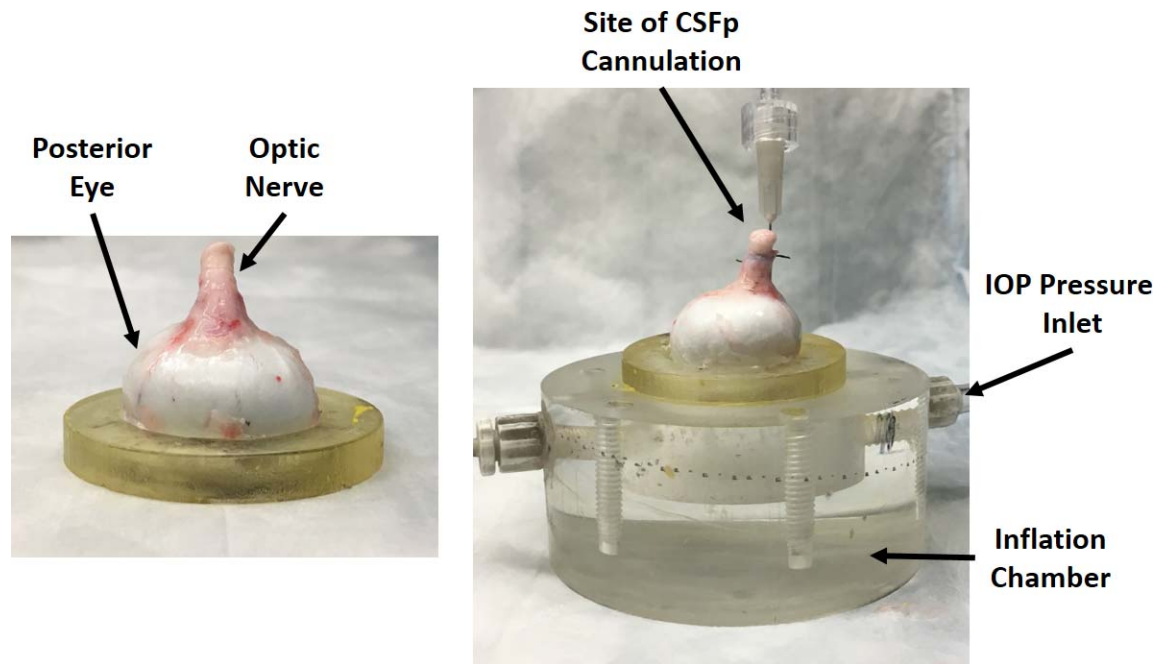
Experimental Protocol

Due to the complex nature of the measurements and limited time available for experiments at the Diamond Light Source synchrotron, specimen preparation was necessarily carried out in advance of measurements. Eyes from female American Yorkshire pigs (weight: 400–600 lbs) were obtained from a local abattoir in Atlanta, Georgia, USA, and were received without orientation information (i.e., OS, OD, or nasal/temporal). Eyes were required to have an intact optic nerve and optic nerve sheath longer than 2 cm. Specimens were prepared using a previously established protocol.[24] Briefly, eyes were cleaned of extraorbital fat and muscles, and the cornea and globe contents (iris, lens, vitreous, retina, and choroid) were removed, leaving an isolated scleral shell. The isolated posterior scleral shell was then sealed onto a resin holder at the corneal-scleral limbus (Fig. 1) by using cyanoacrylate glue. Samples were wrapped in saline-soaked gauze and frozen at −20°C. Previous research showed that this approach had minor effects on scleral mechanics undergoing inflation testing.[25] After preparation, frozen samples were shipped overnight to the United Kingdom for imaging at the Diamond Light Source synchrotron in dry ice and immediately placed in a freezer upon arrival. Prior to imaging, all samples were first refrigerated at 4°C and then thawed at 21°C. The previously prepared posterior scleral shells mounted on resin holders were secured onto a pressure chamber filled with isotonic phosphate-buffered saline (PBS). This pressure chamber was attached to a PBS reservoir which allowed us to control IOP by adjusting reservoir height.

To mimic the effects of CSFp, we inserted the tip of a 23-G blunt cannula into the subarachnoid space. Briefly, 0.5 cm of the optic nerve sheath was peeled away from the optic nerve, and the cannula tip was inserted into the subarachnoid space. To secure the cannula, a silk suture was tightened around the outside of the optic nerve sheath, so the tissue was compressed against the cannula. This ensured that fluid could flow into the subarachnoid space while preventing leakage out of the incised end of the optic nerve. This cannula was connected to a Luer fitting (Cole-Parmer, Vernon Hills, IL, USA) and to a second PBS reservoir to hydrostatically control CSFp. The cannula was supported in the anterior-posterior direction to ensure the weight of the cannula itself did not impact RLNT deformation. Otherwise, the transected end of the optic nerve was free to move and deform throughout the experiment. Specimens were then immersed in a PBS bath to maintain hydration and environmental temperature during testing (a thermocouple placed in the PBS bath showed no change of temperature during testing). Eyes were inflated to an IOP of 15 mm Hg, to represent a physiological relevant value of IOP. A CSFp of 4 mm Hg was applied for 20 minutes to ensure the absence of leakage and to precondition the sample before starting measurements. Based on earlier work, no further preconditioning tests were performed.[25] Several eyes failed for various technical issues (time constraints or leakage leading to an inability to maintain IOP or CSFp), so that this work reports data from $n = 3$ eyes.

The effects of CSFp on the 3-dimensional deformations of the lamina cribrosa and RLNT were measured using a PC μCT beamline I12 unit (Diamond Light Source).[26] The experimental protocol for PC μCT was described previously.[24] The eye specimen was mounted on a turntable. The X-ray beam was directed toward the ONH region and centered on the lamina cribrosa. The phase shift caused by the interaction of the X-rays with the tissues of the ONH was transformed into intensity variations and recorded using a charge-coupled device detector with a resolution of 3.2 μm per pixel. Projections, 3600, with an exposure time of 5 ms each were acquired in the ONH region. The total scan time at each CSFp was roughly 90 s, and the field of view was approximately $7 \times 7 \times 7$ mm³. After images centered at the lamina cribrosa were recorded, a second scan was acquired at the same CSFp with the image sequence centered on the RLNT, 4.5 mm posterior to the ONH.

The PC μCT scan pairs, one centered on the lamina cribrosa and one centered on the RLNT, were recorded at 4 sequential

FIGURE 1. Experimental preparation for imaging of porcine ONH and RLNT. The posterior eye was first glued to a ring (*left*) and then secured to an inflation chamber (*right*) that allowed hydrostatic control of IOP, set to 15 mm Hg throughout the duration of the experiment. A blunt cannula was gently inserted into the subarachnoid space to allow CSFp to also be controlled hydrostatically. The posterior eye was then placed in a tissue chamber (*not shown*) to maintain hydration during the experiment and was imaged. At each CSFp (4, 10, 20, and 30 mm Hg), two PC μCT image sets were collected: one at the ONH to capture the lamina cribrosa and one within the RLNT.

steps of elevating CSFp: 4, 10, 20, and 30 mm Hg. The reference CSFp lays within the physiological range measured in pigs and human patients.[27] Specifically, the mean ± SD CSFp measured in vivo in the pig is 7 ± 4 mm Hg, and between −4 and 10 mm Hg for humans in the upright and supine ranges, respectively.[28-30] Furthermore, 4 mm Hg was the minimum CSFp that ensured that fluid surrounded the optic nerve, which in turn, allowed us to reliably distinguish pia mater from dura mater, required for tracking deformations within the optic nerve as CSFp changed. Our second pressure step was still within the normal physiologic range, whereas 20 and 30 mm Hg represented elevated CSFp values typical for astronauts after returning to earth and for IIH patients (CSFp ≥ 15 mm Hg),[16,31] while remaining below the upper limits of CSFp reported in IIH patients (CSFp > 40 mm Hg).[31] At each pressure step, the specimen was allowed to equilibrate for 15 minutes prior to imaging to ensure the tissue had reached a steady state and to minimize motion due to creep. Intraocular pressure was held constant at 15 mm Hg throughout all scans. Tomographic images were reconstructed by in-house codes including phase retrieval,[32,33] ring artifact removal,[34] filtered-back projection,[35] and background correction.[36] Afterwards, reconstructed images were downsampled to an effective isotropic voxel size of 6.4 μm to reduce file sizes for subsequent analysis.

Digital Volume Correlation

The CSFp-induced deformation of the lamina cribrosa and RLNT were computed using digital volume correlation (DVC), which operates on full 3D image volumes. We recently characterized the use of this method to study lamina cribrosa deformation in the porcine eye due to changes in IOP.[24] Briefly, image volumes for each of the lamina cribrosa and RLNT acquired at CSFp values of 10, 20, and 30 mm Hg were correlated with the corresponding image volumes acquired at

4 mm Hg, using commercially available software (DaVis version 8.1.3: LaVision, GmbG, Goettingen, Germany). We then performed DVC on subvolumes (20 × 20 × 20 voxels), with a 75% overlap, settings that were previously estimated to result in a strain accuracy of 20 microstrain in the porcine lamina cribrosa.[25] These displacements were smoothed using cubic splines and then used to determine the 6 independent components of the spatially varying Green-Lagrange strain tensor at each elevated CSFp level. The Green-Lagrange strain is a 3D measurement of tissue deformation. In addition, the software computed a correlation value for each subvolume image, which is a measurement of the confidence of the strain values. For our analysis, we removed regions where the correlation value was <0.7 to ensure strains included in our analysis were not due to image noise or distortion; this threshold was determined to be suitable in our early experiments.[24] This typically resulted in 10% to 20% of the tissue having strain values that were excluded from analysis.

The Green-Lagrange strain tensor can be decomposed into 3 principal strains representing tissue deformation in three mutually perpendicular directions. Here, we focused on the first principal strain (representing tissue extension) and third principal strain (representing compression). We focused on these two principal strain components because they represent the largest magnitude of strains experienced at each location and thus presumably are related to the biomechanical insult experienced by cells in those regions. We examined the change in principal strain distributions of the lamina cribrosa and RLNT as a function of CSFp. Strain distributions between each subsequent CSFp step were compared by using a paired Wilcoxon signed rank test ($P < 0.05$).

RESULTS

We were able to clearly identify the lamina cribrosa in the ONH, as distinct from the surrounding neural and connective

Lamina Cribrosa   **Retro-laminar Neural Tissue**
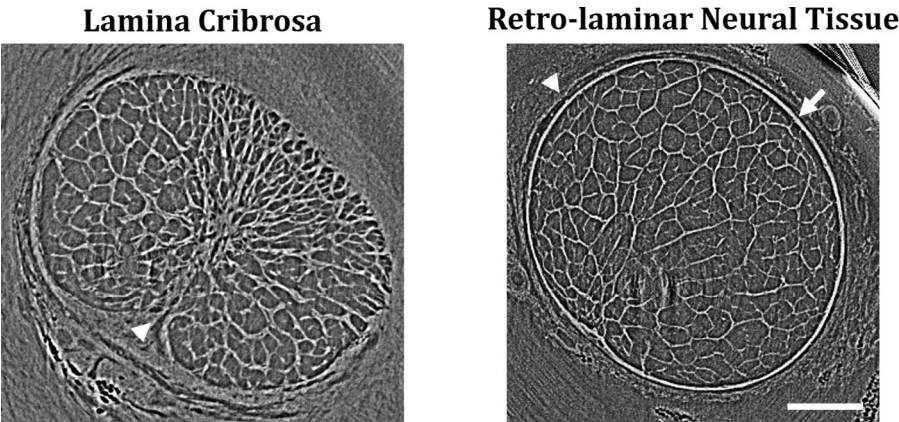
FIGURE 2. Representative cross-sectional images of the lamina cribrosa (*left*) and RLNT (*right*), captured from a 3D PC μCT image set of a porcine eye. We can clearly observe the relatively dense collagen beams in the lamina cribrosa. The lamina cribrosa of the porcine eye also contains a ventral groove (*arrowhead*) where the retinal blood vessels enter the optic nerve. The RLNT contains thinner collagenous structures throughout its cross-section. The RLNT is also encapsulated by the pia mater (*arrow*), which appears as a thin, bright white band around the entire circumference of the optic nerve. The dura mater (*arrowhead*) is also visible. A small imaging artifact is visible near the center of the right image. *Scale bar*: 1 mm.

tissue. The lamina cribrosa of the porcine eye is less circular in cross-section than the posterior neural tissue and contains a thick, dense collagen matrix (Fig. 2). The RLNT, imaged in our second scan, was more circular in cross-section than the lamina cribrosa, with thinner collagen fibers and dense pia mater surrounding the neural tissue (Fig. 2).

Our results showed that increasing CSFp caused optic nerve sheath distention (Fig. 3) and changes in the distributions of the first, second, and third principal strains in both the lamina cribrosa and the RLNT ($P < 0.001$ for all pressure steps in each tissue) (Fig. 4). The strains in both the lamina cribrosa and the RLNT were spatially nonuniform.
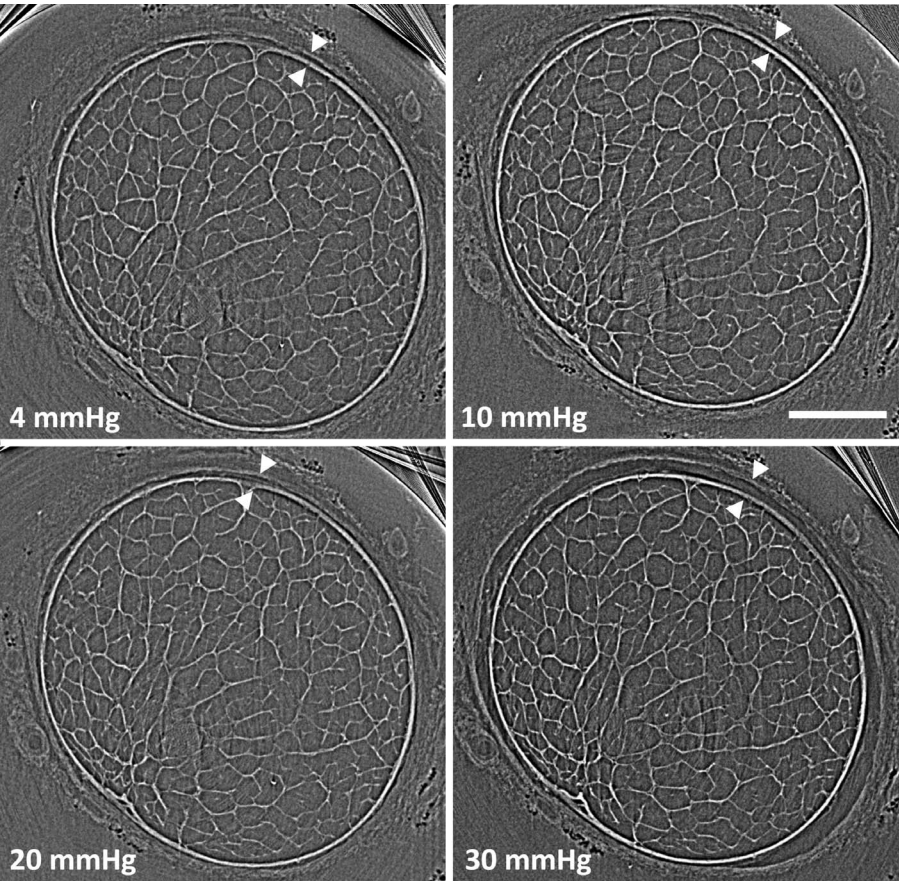
FIGURE 3. Cross-sectional images of a single RLNT and optic nerve sheath at increasing levels of CSFp. It is evident that the subarachnoid space (*arrowheads*) expands as CSFp increases from 4 to 30 mm Hg. Interestingly, this expansion was not spatially uniform. *Scale bar*: 1 mm.
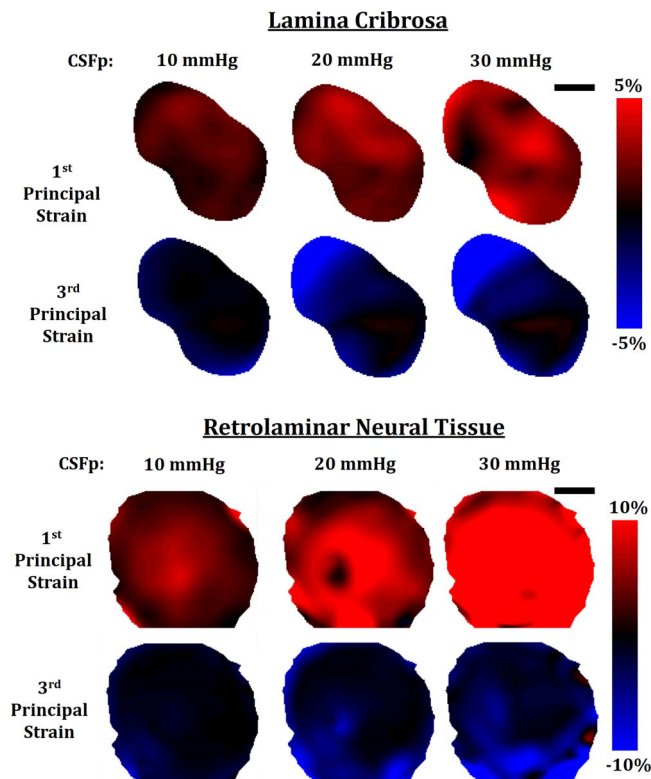
Lamina Cribrosa

Retrolaminar Neural Tissue

FIGURE 4. Contour maps of the first and third principal strains in the lamina cribrosa (*top panel*) and RLNT (*bottom panel*) for different CSFp levels compared with the situation obtained when CSFp was 4 mm Hg. Tissue extension (tension) is shown in *red*, and compression is shown in *blue*. An increase in the tension and compression within the lamina cribrosa and RLNT is observed as CSFp is elevated. The first and third principal strains were larger in the RLNT than in the lamina cribrosa (note differences in color scale bar). *Scale bar*: 1 mm.

Inter-eye variations in average strain magnitude as CSFp increased were small. However, the spatial distribution of these strains within the lamina cribrosa differed between eyes. One eye had higher strain near the ventral groove (inferior region) while the other eyes experienced higher strains superiorly. When we examined the probability density functions of the principal strains, we found that elevating CSFp increased the first principal strain distributions (i.e., a shift to the right) and third principal strain distributions (i.e., a shift to the left [Supplementary Fig. S1]), implying that extreme values of the principal strains increased as CSFp was elevated. Importantly, strain changes were most pronounced in the RLNT.

To better characterize how these strain distributions changed as a function of CSFp, we also calculated the mean and peak values of the first and third principal strains at each CSFp step. The mean strain was simply the mean value over the entire tissue region of interest, whereas the peak strain was defined as the 95th percentile (5th percentile) value from the histogram of the first (third) principal strain, respectively. This approach has been described elsewhere.[23] These peak strains are of interest because they presumably induce the maximum mechanobiological effects in tissues.[21]

Within the lamina cribrosa, the mean first principal strain increased from 2.51% to 4.43%, and the mean third principal strain changed from −1.79% to −3.53% as CSFp increased from 10 to 30 mm Hg. Note that because the third principal strain is negative, this decrease in the third principal strain implies a 65% increase in the magnitude of this strain. The corresponding values within the RLNT were an increase from 4.69% to 9.51% in the mean first principal strain and a change from −3.10% to −9.06% in the mean third principal strain (Fig. 5). Relative to the lamina cribrosa, the magnitudes of the mean principal strains in the RLNT were roughly 2- to 2.5-fold higher. The same trend was observed in the peak strains within the lamina cribrosa and RLNT (Fig. 5).

DISCUSSION

Here, we report that elevating CSFp increased the principal strains (deformations) within both the lamina cribrosa and the
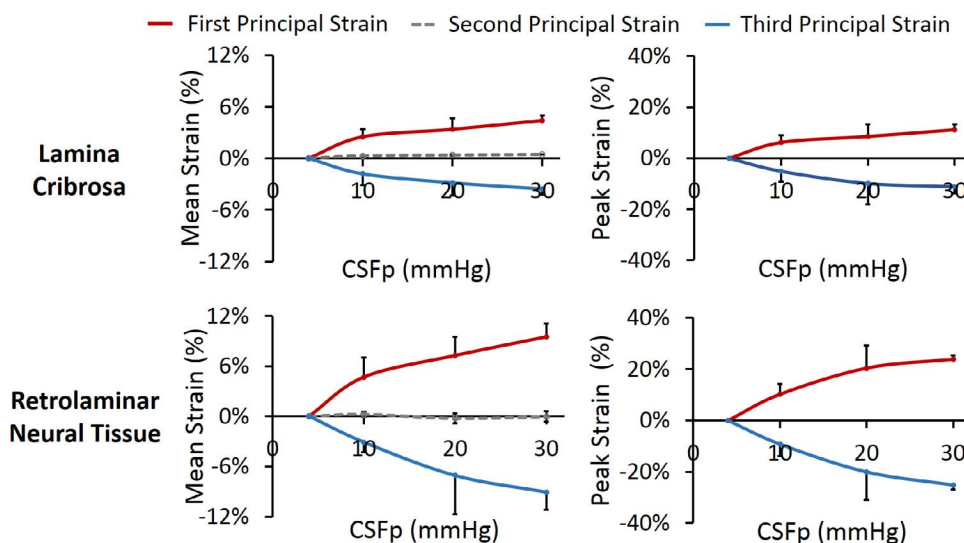

FIGURE 5. The mean (*left column*) and peak (5th/95th percentile [*right column*]) principal strains in the lamina cribrosa (*top row*) and RLNT (*bottom row*) are shown. Data are average ± SD of the three samples. Note the differences in vertical axis scales between the left and right columns. The mean and peak principal strains increased as CSFp increased in both the lamina cribrosa and the RLNT. See Results section for definitions of how the mean and peak strains were determined. Note that the concept of peak strain magnitude for the second principal strain is undefined so that there are no dashed lines in the graphs in the right column.

RLNT, with the effects being more pronounced in the RLNT. Increased strain on the RGCs and cells within the lamina cribrosa are potential contributors to axonal transport blockage and eventually the loss of retinal ganglion cells (RGCs).[37–40] Currently, most work examining ONH mechanobiology has focused on how elevations in IOP influence strains within the lamina cribrosa.[25,38,41–45] A previous study, also using PC μCT scanning of porcine eyes, investigated the effect of IOP on lamina cribrosa deformation. That study found that elevating IOP from 6 to 30 mm Hg increased mean first principal strain in the lamina cribrosa by 5.5%.[25] In the present study, we found that elevating CSFp from 4 to 30 mm Hg increased the mean first principal strain in the lamina by 4.43%, similar to the effects due to elevating IOP from 6 to 30 mm Hg. However, considering the mean third principal strain, elevating IOP resulted in mean strains in the lamina cribrosa of −15%,[25] whereas elevating CSFp produced mean third principal strains of only −3.5%. In other words, elevating IOP may have a proportionately larger impact on the compression experienced in the lamina cribrosa than does elevating CSFp. This may be related to several key differences between the effects of IOP and CSFp: notably, CSF is contained within the optic nerve sheath within the subarachnoid space, so that CSFp and retrolaminar tissue pressure act only on the posterior globe at the optic nerve head and not on the entire corneoscleral shell. Nonetheless, it is important to understand that CSFp influences lamina cribrosa biomechanics.

However, the situation was different when we considered the RLNT, where we found a dramatic increase in the first and third principal strains due to an elevation of CSFp. Elevated strains in the RLNT likely have a biomechanical impact, for example, increased tension and compression can cause mechanical insult directly to the RGC axons, which may increase the risk of RGC loss. Additional research of the mechanobiology of the RLNT is needed to better understand the impact of these observations.

These results have several potential clinical implications. First, the finding that increased CSFp caused increases in both the first and third principal strains in the lamina cribrosa and the RLNT is consistent with radiographic evidence of optic nerve axial elongation and radial compression, respectively, in IIH patients.[46,47] Furthermore, the optic nerve sheath distention seen in our experiments (Fig. 3) is also consistent with findings in both patients with IIH and in astronauts with VIIP syndrome.[16,46–49] These changes in the optic nerve and optic nerve sheath would likely result in ocular protrusion if it were not for the fact that the globe is yoked by the rectus muscles and check ligaments. Because anterior displacement is restricted by the muscles and ligaments, these optic nerve and sheath changes which result in the displacement of the ONH and RLNT may contribute to posterior globe flattening commonly seen in both IIH and VIIP syndrome.[46,47] Finally, these results bring attention to the issue of CSFp and the translaminar pressure differences in glaucoma patients. Current thinking is that a change in the translaminar pressure difference may be an independent risk factor for the development of glaucoma and its progression,[13,50] with reduction of the translaminar pressure difference being protective of RGC axons. Here, our experimental design and examination of a single IOP limits our ability to assess changes in the translaminar pressure differences. However, we did find that CSFp directly impacted strains in the lamina cribrosa and more so in the RLNT. The biological sequelae of these mechanical effects are largely unknown and merit additional studies.

Earlier in vivo work by Morgan et al.[20] in a canine model showed that elevating CSFp can lead to displacement of ONH tissues (see the introduction[20]). Those authors found that CSFp changes were very influential in affecting the topography of the vitroretinal interface as measured by scanning laser ophthalmoscopy, whereas our results showed more modest effects on strains in the lamina cribrosa (i.e., compared to the effect of changing IOP). However, this comparison needs to be considered carefully. Most notably, Morgan et al.[20] reported deformations, whereas in the present study, we reported strains. As discussed above, these are different quantities, and so the results of our study are not necessarily inconsistent with those of the study by Morgan et al.[20] We attempted to replicate the experiments of Morgan et al.[20] by extracting deformations of the vitroretinal interface from our μCT scans, which would have enabled a more direct comparison. Unfortunately, we were unable to do so due to a variety of technical issues, and this would be a worthwhile consideration in future experiments. Sigal et al. (*IOVS* 2016;57:ARVO E-Abstract 1794) examined the effect of elevating CSFp in the nonhuman primate model, using optical coherence tomography to determine the effects of IOP and CSFp on the lamina cribrosa (Tran H, et al. *IOVS* 2015;56; ARVO E-Abstract 6150; Wang B, et al. *IOVS* 2015;56; ARVO E-Abstract 3979). They found that both IOP and CSFp affected strains in the anterior lamina cribrosa, with such strains exceeding 20% for certain combinations of IOP and CSFp. Interestingly, although elevating CSFp in most animals expanded the scleral canal and moved the lamina cribrosa anteriorly, in a minority of cases it had the opposite impact. Thus, there appears to be a degree of specimen-dependent impact on how CSFp influences ONH deformation.

Importantly, the above-described experimental studies collectively illustrate how CSFp has an impact on displacements and deformations within the ONH. A recently developed computational model by our group also examined how CSFp impacts strains within the ONH. This computational model predicted that elevating CSFp to 20 mm Hg would increase the strains within the RLNT but would decrease strains within the lamina cribrosa,[23] which is different than our experimental observations of lamina cribrosa strains. There are several potential reasons for these differences. First, the computational models were based on human ocular anatomy, whereas our experiments were carried out in a porcine model, which may play a role in how CSFp influences strain at the ONH. The potential importance of species-specific anatomic effects is consistent with the observations by Sigal et al. (*IOVS* 2016;57:ARVO E-Abstract 1794) that different eyes may respond differently to elevated CSFp.

However, we were dissatisfied with this explanation and returned to our numerical simulations, simulating a higher range of CSFps than we had originally done.[23] We found a complex outcome: after the initial decrease in lamina cribrosa strain at a CSFp of 20 mm Hg, tissue strains began to increase as CSFp further increased (Supplementary Figs. S1–S2). This nonmonotonic behavior may partially reconcile our experimental and computational results. For example, it is possible that the step increases of CSFp in our experiment were too large to detect this nonmonotonic behavior, especially in view of possible estimations of connective tissue mechanical properties needed for modeling (see below).

Nonetheless, it is likely that CSFp plays a more important role in lamina cribrosa deformation than originally predicted in our computational models. For example, the strain magnitudes predicted by the computational models were 4-fold lower than those measured experimentally in our study. Computational models tend to underestimate tissue strains on a continuum level compared to micromodels of the lamina cribrosa or experimental results.[24,38] Furthermore, the impact CSFp has in computational models is limited by assumptions about tissue

behavior and simplification of geometries. This is particularly critical for the pia mater, which directly influences the transmission of CSFp to the optic nerve and influences strains in the lamina cribrosa.[23] If our material models overestimate the stiffness of this tissue, there would be a significant impact on the predicted strains from our computational models, including an estimation of the CSFp level at which the lamina cribrosa would begin to experience an increase in strain due to elevated CSFp. For example, the porcine eye has different biomechanical properties compared to the human eye that would influence the level or strain predicted.[51] This outcome points to the importance of species-specific measurement of the material properties of ONH tissues, which is a major experimental challenge. We expect that the experimental data presented in this work will be valuable in verifying the results of more sophisticated computational models.

Study Limitations

This study had several limitations. Most notably, we had a limited sample size. PC μCT imaging relies on access to a synchrotron light source. The high facility cost and demand for time on the machine limits the number of experiments that can be performed. Nonetheless, the intersample variability in strain magnitudes was relatively low. Specifically, across all CSFp levels, we calculated a coefficient of variation for the mean first and third principal strain of 28% and 48%, respectively, within the lamina cribrosa and of 32% and 43% within the RLNT, respectively. Given the natural variability among eyes, we believe these data are robust. Thus, even with our limited sample size, it appears that elevating CSFp has profound effects on the strains in the RLNT and in the lamina cribrosa, both of which may be important for the health of the RGC axons.

Another limitation is that we did not simultaneously alter IOP and CSFp. Previous work found that there is a strong interplay between these pressures and that using our approach would have been beneficial to investigating this interaction (Sigal IA, et al. *IOVS* 2016;57:ARVO E-Abstract 1794).[20] However, due to our limited scan time, we could focus only on the influence of CSFp in this study. In addition, our experimental approach only examined acute elevations of CSFp, while IIH patients or astronauts exposed to microgravity may have chronic elevations in CSFp which may induce remodeling of connective tissues in the ONH and optic nerve sheath. Developing animal or computational models to investigate how chronic exposures to CSFp can alter tissue properties and induce remodeling would be relevant.[52]

We also only examined the impact of CSFp in an ex vivo model on postmortem porcine eyes that were frozen prior to testing. Although it has been shown that freezing has minimal impact on scleral connective tissue biomechanical properties,[25] we were not able to directly assess the impact of freezing on the biomechanical properties of the RLNT. However, it has been shown that postmortem swelling of axons does occur,[53] which indicates our ex vivo condition may not have fully represented the in vivo anatomy. Although an in vivo approach would have been preferred, our imaging approach (PC μCT) made this option impossible. Based on earlier work, we assumed that axon swelling occurred uniformly and induced connective tissue strains that were small compared to the strains we observed due to elevations in CSFp.[25] Another limitation was the use of porcine eyes. Although we would have preferred to perform this experiment using human eyes, we were unable to consistently obtain human eyes with optic nerves that were long enough to cannulate for control of CSFp. Therefore, we chose to use porcine eyes because their ONH geometry is broadly similar to

that of humans and because eyes were available with sufficiently long optic nerves. However, as quadrupeds, porcine CSFp likely does not fluctuate to the same degree as in humans, who alternate between a supine and upright position.[30] Thus, using this animal model has limitations; however, previous work in canine and porcine models still provides insight into how IOP and CSFp influence the biomechanical environment at the ONH.[5,20,24]

Last, digital correlation approaches are subject to limitations in resolving small deformation.[24,54] Fortunately, the deformations in the lamina cribrosa and RLNT in this study varied between 4% and 20%, which is orders of magnitude larger than the strains that DVC can resolve.[25] Therefore, we are confident that our strain measurements were not limited by the resolution of DVC.

In conclusion, we were able to use PC μCT imaging and DVC to experimentally visualize and quantify the deformations of the lamina cribrosa and RLNT as CSFp increased. We found that strain (i.e., the tension and compression) experienced in the lamina cribrosa and RLNT increase as CSFp is elevated and that CSFp induced larger strains on the RLNT than in the lamina cribrosa. These elevated strains may contribute to the loss of RGC axons under pathologic conditions.

Disclosure: **A.J. Feola**, None; **B. Coudrillier**, None; **J. Mulvihill**, None; **D.M. Geraldes**, None; **N.T. Vo**, None; **J. Albon**, None; **R.L. Abel**, None; **B.C. Samuels**, None; **C.R. Ethier**, None

References

1. Ethier CR, Johnson M, Ruberti J. Ocular biomechanics and biotransport. *Annu Rev Biomed Eng*. 2004;6:249–73.

2. Downs JC, Roberts MD, Burgoyne CF. Mechanical environment of the optic nerve head in glaucoma. *Optom Vis Sci*. 2008;85(6):425–35.

3. Bellezza AJ, Rintalan CJ, Thompson HW, et al. Anterior scleral canal geometry in pressurised (IOP 10) and non-pressurised (IOP 0) normal monkey eyes. *Br J Ophthalmol*. 2003;87: 1284–1290.

4. Roberts MD, Liang Y, Sigal IA, et al. Correlation between local stress and strain and lamina cribrosa connective tissue volume fraction in normal monkey eyes. *Invest Ophthalmol Vis Sci*. 2010;51:295–307.

5. Morgan WH, Yu DY, Alder VA, et al. The correlation between cerebrospinal fluid pressure and retrolaminar tissue pressure. *Invest Ophthalmol Vis Sci*. 1998;39:1419–1428.

6. Burgoyne CF. A biomechanical paradigm for axonal insult within the optic nerve head in aging and glaucoma. *Exp Eye Res*. 2011;93:120–132.

7. Bellezza AJ, Rintalan CJ, Thompson HW, et al. Deformation of the lamina cribrosa and anterior scleral canal wall in early experimental glaucoma. *Invest Ophthalmol Vis Sci*. 2003;44: 623–637.

8. Girard MJ, Suh JK, Bottlang M, Burgoyne CF, Downs JC. Biomechanical changes in the sclera of monkey eyes exposed to chronic IOP elevations. *Invest Ophthalmol Vis Sci*. 2011; 52:5656–5669.

9. Sigal IA, Flanagan JG, Tertinegg I, Ethier CR. Finite element modeling of optic nerve head biomechanics. *Invest Ophthalmol Vis Sci*. 2004;45:4378–4387.

10. Bellezza AJ, Hart RT, Burgoyne CF. The optic nerve head as a biomechanical structure: initial finite element modeling. *Invest Ophthalmol Vis Sci*. 2000;41:2991–3000.

11. Sigal IA, Bilonick RA, Kagemann L, et al. The optic nerve head as a robust biomechanical system. *Invest Ophthalmol Vis Sci*. 2012;53:2658–2667.

12. Morgan WH, Yu DY, Cooper RL, et al. The influence of cerebrospinal fluid pressure on the lamina cribrosa tissue pressure gradient. *Invest Ophthalmol Vis Sci*. 1995;36:1163–1172.

13. Berdahl JP, Allingham RR, Johnson D H. Cerebrospinal fluid pressure is decreased in primary open-angle glaucoma. *Ophthalmology*. 2008;115;763–768.

14. Ren R, Jonas JB, Tian G, et al. Cerebrospinal fluid pressure in glaucoma: a prospective study. *Ophthalmology*. 2010;117: 259–266.

15. Morgan WH, Yu DY, Balaratnasingam C. The role of cerebrospinal fluid pressure in glaucoma pathophysiology: the dark side of the optic disc. *J Glaucoma*. 2008;17:408–413.

16. Mader TH, Gibson CR, Pass AF, et al. Optic disc edema, globe flattening, choroidal folds, and hyperopic shifts observed in astronauts after long-duration space flight. *Ophthalmology*. 2011;118:2058–2069.

17. Kramer LA, Sargsyan AE, Hasan KM, Polk JD, Hamilton DR. Orbital and intracranial effects of microgravity: findings at 3-T MR imaging. *Radiology*. 2012;263:819–827.

18. Mader TH, Gibson CR, Pass AF, et al. Optic disc edema in an astronaut after repeat long-duration space flight. *J Neuro-ophthalmol*. 2013;33:249–255.

19. Taibbi G, Cromwell RL, Kapoor KG, Godley BF, Vizzeri G. The effect of microgravity on ocular structures and visual function: a review. *Surv Ophthalmol*. 2013;58:155–163.

20. Morgan WH, Chauhan BC, Yu DY, et al. Optic disc movement with variations in intraocular and cerebrospinal fluid pressure. *Invest Ophthalmol Vis Sci*. 2002;43;3236–3242.

21. Beckel JM, Argall AJ, Lim JC, et al. Mechanosensitive release of adenosine 5′-triphosphate through pannexin channels and mechanosensitive upregulation of pannexin channels in optic nerve head astrocytes: a mechanism for purinergic involvement in chronic strain. *Glia*. 2014;62:1486–1501.

22. Shao Y, Tan X, Novitski R, et al. Uniaxial cell stretching device for live-cell imaging of mechanosensitive cellular functions. *Rev Sci Instrum*. 2013;84:114304.

23. Feola AJ, Myers JG, Raykin J, et al. Finite element modeling of factors influencing optic nerve head deformation due to intracranial pressure. *Invest Ophthalmol Vis Sci*. 2016;57: 1901–1911.

24. Coudrillier B, Campbell IC, Read AT, et al. Effects of peripapillary scleral stiffening on the deformation of the lamina cribrosa. *Invest Ophthalmol Vis Sci*. 2016;57:2666–2677.

25. Coudrillier B, Geraldes DM, Vo NT, et al. Phase-contrast micro-computed tomography measurements of the intraocular pressure-induced deformation of the porcine lamina cribrosa. *IEEE Trans Med Img*. 2016;35:988–999.

26. Drakopoulos M, Connolley T, Reinhard C, et al. I12: the Joint Engineering, Environment and Processing (JEEP) beamline at Diamond Light Source. *J Synchrotron Radiat*. 2015;22:828–838.

27. Kaiser GM, Fruhauf NR. Method of intracranial pressure monitoring and cerebrospinal fluid sampling in swine. *Lab Anim*. 2007;41:80–85.

28. Alperin N, Lee SH, Sivaramakrishnan A, Hushek SG. Quantifying the effect of posture on intracranial physiology in humans by MRI flow studies. *J Magn Reson Imaging*. 2005; 22:591–596.

29. Magnaes B. Body position and cerebrospinal fluid pressure. Part 1: clinical studies on the effect of rapid postural changes. *J Neurosurg*. 1976;44:687–697.

30. Magnaes, B. Body position and cerebrospinal fluid pressure. Part 2: clinical studies on orthostatic pressure and the hydrostatic indifferent point. *J Neurosurg*. 1976;44:698–705.

31. Kattah JC, Pula JH, Mejico LJ, et al. CSF pressure, papilledema grade, and response to acetazolamide in the Idiopathic Intracranial Hypertension Treatment Trial. *J Neurol*. 2015; 262:2271–2274.

32. Atwood RC, Bodey AJ, Price SW, Basham M, Drakopoulos M. A high-throughput system for high-quality tomographic reconstruction of large datasets at Diamond Light Source. *Philos Trans A Math Phys Eng Sci*. 2015;373.

33. Paganin D, Mayo SC, Gureyev TE, Miller PR, Wilkins SW. Simultaneous phase and amplitude extraction from a single defocused image of a homogeneous object. *J Microsc*. 2002; 206:33–40.

34. Raven C. Numerical removal of ring artifacts in micro-tomography. *Rev Sci Instrum*. 1998;69:2.

35. Titarenko V, Bradley R, Martin C, Withers PJ, Titarenko S. Regularization methods for inverse problems in x-ray tomography. *Proc SPIE*. 2010;7804:78040Z.

36. Vo NT, Drakopoulos M, Atwood RC, Reinhard C. Reliable method for calculating the center of rotation in parallel-beam tomography. *Opt Express*. 2014;22:19078–19086.

37. Minckler DS, Bunt AH, Johanson GW. Orthograde and retrograde axoplasmic transport during acute ocular hypertension in the monkey. *Invest Ophthalmol. Vis Sci*. 1997;16: 426–441.

38. Sigal IA, Ethier CR. Biomechanics of the optic nerve head. *Exp Eye Res*. 2009;88:799–807.

39. Hernandez MR. The optic nerve head in glaucoma: role of astrocytes in tissue remodeling. *Prog Retin Eye Res*. 2000;19: 297–321.

40. Anderson DR, Hendrickson A. Effect of intraocular pressure on rapid axoplasmic transport in monkey optic nerve. *Invest Ophthalmol*. 1974;13:771–783.

41. Sigal IA, Grimm JL, Jan NJ, et al. Eye-specific IOP-induced displacements and deformations of human lamina cribrosa. *Invest Ophthalmol Vis Sci*. 2014;55:1–15.

42. Sigal IA, Flanagan JG, Tertinegg I, Ethier CR. Predicted extension, compression and shearing of optic nerve head tissues. *Exp Eye Res*. 2007;85:312–322.

43. Strouthidis NG, Fortune B, Yang H, Sigal IA, Burgoyne CF. Effect of acute intraocular pressure elevation on the monkey optic nerve head as detected by spectral domain optical coherence tomography. *Invest Ophthalmol Vis Sci*. 2011;52: 9431–9437.

44. Yang H, Downs JC, Sigal IA, et al. Deformation of the normal monkey optic nerve head connective tissue after acute IOP elevation within 3-D histomorphometric reconstructions. *Invest Ophthalmol Vis Sci*. 2009;50:5785–5799.

45. Yang H, Thompson H, Roberts MD, et al. Deformation of the early glaucomatous monkey optic nerve head connective tissue after acute IOP elevation in 3-D histomorphometric reconstructions. *Invest Ophthalmol Vis Sci*. 2011;52:345–363.

46. Mashima Y, Oshitari K, Imamura Y, et al. High-resolution magnetic resonance imaging of the intraorbital optic nerve and subarachnoid space in patients with papilledema and optic atrophy. *Arch Ophthalmol*. 1996;114:1197–1203.

47. Brodsky MC, Vaphiades M. Magnetic resonance imaging in pseudotumor cerebri. _Ophthalmology_. 1998;105:1686–1693.

48. Nelson ES, Mulugeta L, Myers JG. Microgravity-induced fluid shift and ophthalmic changes. _Life (Basel)_. 2014;4:621–665.

49. Raykin J, Forte TE, Wang R, et al. Characterization of the mechanical behavior of the optic nerve sheath and its role in spaceflight-induced ophthalmic changes. _Biomech Model Mechanobiol_. 2017;16:33–43.

50. Fleischman D, Allingham RR. The role of cerebrospinal fluid pressure in glaucoma and other ophthalmic diseases: a review. _Saudi J Ophthalmol_. 2013;27:97–106.

51. Mortazavi AM, Simon BR, Stamer WD, Vande Geest JP. Drained secant modulus for human and porcine peripapillary sclera using unconfined compression testing. _Exp Eye Res_. 2009;89: 892–897.

52. Frankfort BJ, Khan AK, Tse DY, et al. Elevated intraocular pressure causes inner retinal dysfunction before cell loss in a mouse model of experimental glaucoma. _Invest Ophthalmol Vis Sci_. 2013;54:762–770.

53. Thanos S, Rohrbach JM, Thiel HJ. Postmortem preservation of ganglion cells in the human retina. A morphometric investigation with the carbocyanine dye DiI. _Retina_. 1991; 11:318–327.

54. Coudrillier B, Tian J, Alexander S, et al. Biomechanics of the human posterior sclera: age- and glaucoma-related changes measured using inflation testing. _Invest Ophthalmol Vis Sci_. 2012;53:1714–1728.

Investigative Ophthalmology & Visual Science